Published online 25 May 2020

Nucleic Acids Research, 2020, Vol. 48, No. 12 ***6513–6529***
doi: 10.1093/nar/gkaa435

Macrophage development and activation involve coordinated intron retention in key inflammatory regulators

Immanuel D. Green[1,2,†], Natalia Pinello[1,2,†], Renhua Song[1,2], Quintin Lee[1,2,3], James M. Halstead[1,2], Chau-To Kwok[1,2], Alex C. H. Wong[1,2,4], Shalima S. Nair[5,6,7], Susan J. Clark[5,6], Ben Roediger[2,3], Ulf Schmitz[2,4,8], Mark Larance[9], Rippei Hayashi[10], John E. J. Rasko[2,4,11] and Justin J.-L. Wong[1,2,*]

[1]Epigenetics and RNA Biology Program Centenary Institute, The University of Sydney, Camperdown 2050, Australia, [2]Faculty of Medicine and Health, The University of Sydney, Camperdown 2050, Australia, [3]Immune Imaging Program Centenary Institute, The University of Sydney, Camperdown 2050, Australia, [4]Gene and Stem Cell Therapy Program Centenary Institute, The University of Sydney, Camperdown 2050, Australia, [5]Genomics and Epigenetics Division, Garvan Institute of Medical Research, Darlinghurst 2010, Australia, [6]St. Vincent's Clinical School, UNSW, Sydney 2010, Australia, [7]Kinghorn Centre for Clinical Genomics, Garvan Institute of Medical Research, Darlinghurst 2010, Australia, [8]Computational Biomedicine Laboratory Centenary Institute, The University of Sydney, Camperdown 2050, Australia, [9]Charles Perkins Centre, School of Life and Environmental Sciences, University of Sydney, Camperdown 2006, New South Wales, Australia., [10]The John Curtin School of Medical Research, The Australian National University, ACT 2601, Australia and [11]Cell and Molecular Therapies, Royal Prince Alfred Hospital, Camperdown 2050, Australia

Received March 18, 2020; Revised May 04, 2020; Editorial Decision May 07, 2020; Accepted May 11, 2020

ABSTRACT

Monocytes and macrophages are essential components of the innate immune system. Herein, we report that intron retention (IR) plays an important role in the development and function of these cells. Using Illumina mRNA sequencing, Nanopore direct cDNA sequencing and proteomics analysis, we identify IR events that affect the expression of key genes/proteins involved in macrophage development and function. We demonstrate that decreased IR in nuclear-detained mRNA is coupled with increased expression of genes encoding regulators of macrophage transcription, phagocytosis and inflammatory signalling, including *ID2*, *IRF7, ENG* and *LAT*. We further show that this dynamic IR program persists during the polarisation of resting macrophages into activated macrophages. In the presence of proinflammatory stimuli, intron-retaining *CXCL2* and *NFKBIZ* transcripts are rapidly spliced, enabling timely expression of these key inflammatory regulators by macrophages. Our study provides novel insights into the molecular factors controlling vital regulators of the innate immune response.

INTRODUCTION

Alternative RNA splicing is a major source of transcriptomic and proteomic diversity in eukaryotic cells (1,2). Intron retention (IR) is one mode of alternative splicing that occurs when an intron is not excised and is preserved within mature mRNA. IR is widespread in diverse cell and tissue types, and is conserved across vertebrate species (3,4). IR is now established as a key mechanism of gene expression control during the development, differentiation and activation of several mammalian cell types, particularly in the neuronal and haematopoietic systems (5–12).

As opposed to other modes of alternative splicing, which generally promote the production of new protein isoforms, IR predominately results in post-transcriptional gene repression. As many introns contain premature termination codons (PTCs), their retention in mRNA can facilitate cytoplasmic degradation of transcripts via the nonsense-mediated decay (NMD) pathway (11,13,14). Alternatively, intron-retaining mRNAs may be detained in the nucleus (15). Following appropriate stimulus, these accumulated

*To whom correspondence should be addressed. Tel: +61 286277434; Email: j.wong@centenary.org.au
†The authors wish it to be known that, in their opinion, the first two authors should be regarded as joint First Authors.
Present address: Ben Roediger, Autoimmunity, Transplantation and Inflammation (ATI) Disease Area, Novartis Institutes for BioMedical Research, Basel, Switzerland.

transcripts can undergo constitutive splicing to enable a rapid burst of protein synthesis (7–9,15–17). It is also possible for nuclear-detained, intron-retaining transcripts to be degraded by the RNA exosome, thereby reducing gene expression independent of NMD (12,18,19). Following our first report that IR coupled with NMD regulates normal granulopoiesis (11), IR has also been implicated in the development and function of other haematopoietic cells including erythroblasts, megakaryocytes and T cells (5,9,10). However, the roles of IR during monocyte-to-macrophage differentiation and macrophage activation have not previously been investigated.

Monocytes and macrophages are essential components of the innate immune system (20). Tissue-resident macrophages can be found in all organs where they play critical roles in tissue homeostasis and serve as sentinels of injury and infection (21). During the steady-state, many tissue-resident macrophages undergo self-renewal for their maintenance (20). Alternatively, under inflammatory conditions, circulating monocytes migrate to affected tissues where they differentiate into macrophages. Macrophages contribute to the inflammatory response by producing cytokines and phagocytosing microbial pathogens and cell debris. Resting 'Mϕ' macrophages can be further differentially polarised into 'M1' or 'M2' subclasses, which support a pro- or anti-inflammatory state, respectively (22,23). Classical M1 polarisation occurs following exposure to microbial antigens and cytokines such as interferon-γ (IFN-γ). These specialised cells have an enhanced cytotoxic phenotype and are instrumental in overcoming microbial infections. The molecular mechanisms controlling macrophage development and polarisation are not fully understood.

Here, we sought to determine what role IR plays in regulating the expression of genes important for macrophage differentiation and function. We identified hundreds of genes exhibiting differential IR and gene expression regulation between monocytes and macrophages. Gene ontology analysis reveals that these genes are enriched for functions relevant to monocytes and macrophages. We further showed that nuclear detention of intron-retaining transcripts enables the timely expression of key inflammatory genes. Our study provides novel insights into the molecular mechanisms underpinning gene expression control in macrophages.

MATERIALS AND METHODS

THP-1 cell culture

Human THP-1 monocytic cells were maintained in RPMI medium supplemented with 2 mM L-glutamine, 25 mM HEPES, 10% (v/v) FBS, 1 mM sodium pyruvate, 1% (v/v) non-essential amino acids, and 0.1 mg/ml penicillin/streptomycin at 37°C in the presence of 5% CO_2. Differentiation of THP-1 monocytes into resting, Mϕ-like macrophages was performed as previously described (24). Briefly, cells were plated at a density of 1.5×10^7 cells per 75 cm^2 culture flask containing supplemented RPMI media with 100 nM phorbol-12-myristate 13-acetate (PMA) and 50 μM 2-mercaptoethanol and cultured for 48 h. Polarisation of THP-1-derived Mϕ-like macrophages into M1-like cells was performed as previously described (25). Cells were cultured in freshly supplemented RPMI media with 1 μg/ml lipopolysaccharide (LPS) and 20 ng/ml IFN-γ over 6 h.

Primary human monocyte and macrophage culture

With informed consent and ethics approval from the Human Research Ethics Committee of the Royal Prince Alfred Hospital (protocol number X16-0300), whole blood samples were obtained from three healthy male individuals (Donors N1, N2 and N3). Blood samples were diluted in Hanks' balanced salt solution (HBBS) in a ratio of 1:2. Following addition of Ficoll and gradient separation, peripheral blood mononuclear cells (PBMCs) were isolated and washed. PBMCs were then frozen in cryopreservation medium containing RPMI medium supplemented with 40% (v/v) FBS and 10% (v/v) DMSO and stored in liquid nitrogen. For $CD14^+$ cell selection, PBMCs were thawed and underwent magnetic-activated cell sorting (MACS) separation according to the manufacturers' instructions (Miltenyi Biotec). Briefly, cells were stained with anti-CD14 phycoerythrin (PE, BioLegend) and anti-PE MicroBeads. Cells were then placed into LS columns and underwent MACS separation. Labelled $CD14^+$ monocytes were collected following washing in phosphate-buffered saline.

Purified monocytes were maintained in RPMI medium supplemented with 2 mM L-glutamine, 25 mM HEPES, 20% (v/v) FBS, and 0.1 mg/ml penicillin/streptomycin at 37°C in the presence of 5% CO_2. Monocytes were differentiated into macrophages using 100 ng/ml M-CSF (PeproTech) for 7 days, with culture media being replaced every 3 days. Following differentiation, macrophages were further polarised to a proinflammatory phenotype using 100 ng/ml LPS and 50 ng/ml IFN-γ for 8 h.

Flow cytometry

Flow cytometry analysis to confirm the differentiation of THP-1 monocytes into Mϕ-like macrophages was performed with anti-CD11b conjugated to allophycocyanin (APC, BioLegend) and anti-CD44 conjugated to phycoerythrin (PE, BD Biosciences) staining. To confirm the polarisation of THP-1 macrophages into M1-like cells, anti-CD38 conjugated to PE-Cy7 (BioLegend) and anti-CD80 conjugated to V450 (BD Biosciences) were used. Cell viability was determined by staining cells with 0.5 μg/ml 4′,6-diamidino-2-phenylindole dihydrochloride (DAPI; Invitrogen). Acquisition was performed using a BD FACSCanto™ II and a BD FACSFortessa™ II (BD Biosciences) and data were analysed using FlowJo software (BD Biosciences).

RNA extraction and RT-qPCR

RNA extraction was performed using TRIzol® (Invitrogen) according to the manufacturers' instructions. RNA quality and quantity were determined using the RNA 6000 Nano kit on a Bioanalyzer (Agilent Technologies). All RNA samples have RIN value of >9. RT-qPCR was performed on cDNA generated from 1–1.5 μg DNaseI-treated total RNA using SuperScript® III First-Strand Synthesis

System (Invitrogen), according to the manufacturers' instructions. To measure mRNA expression, cDNA synthesis was primed using oligo-dT_{18} (Bioline). To measure promoter upstream transcript (PROMPT) expression, random hexamers (Bioline) were used. RT-qPCR reactions were performed in 20 μl volumes containing 1X iQ™ SYBR® Green Supermix (Bio-Rad) and 0.3 μM of the respective forward and reverse primers. Samples were amplified and analysed using the CFX96™ Real Time PCR Machine (Bio-Rad). Cycling conditions were: 95 °C for 6 min, followed by 40 cycles at 95 °C for 30 s, the respective annealing temperature (Supplementary Table S1) for 30 s, and extension at 72 °C for 30 s. All qPCR primers used are detailed in Supplementary Table S1. Levels of IR were measured in transcripts amplified using primers spanning exon–intron normalised to amplicons spanning adjacent exons as previously described (11). For the measurement of spliced transcript expression, *B2M* was used as the normalisation control for cDNA input. For each sample, a corresponding control without reverse transcriptase was used to exclude the possibility of DNA contamination. Fold change was calculated using the ΔΔCT method as previously reported (11).

Illumina mRNA Sequencing and Bioinformatics

Poly-A-enriched mRNA libraries were prepared from 2 μg of TURBO™ DNase-treated, total RNA using the TruSeq® Stranded Library Preparation Kit (Illumina), according to the manufacturers' instructions. mRNA sequencing was performed on each cell population in triplicates by Novogene (China). A total of 100 million paired-end strand-specific reads were sequenced per sample on an Illumina HiSeq® 2500 Platform. mRNA sequence reads were mapped to the human genome (hg38 assembly) using STAR (26). IR was quantified using IRFinder (27). Briefly, IR levels were measured using the IR ratio metric (an intron's abundance divided by the sum of the intron and flanking exon abundances). Introns with an IR ratio <0.1 in both conditions were excluded from further analyses. Differential gene expression was measured using DESeq2 (28). Primary monocyte and macrophage mRNA sequencing data was retrieved from the Sequence Read Archive (SRA) database under accession number SRP139891 of BioProject PRJNA449980 (29).

Whole-genome bisulphite sequencing (WGBS) was performed on a HiSeq X Ten platform (Illumina) following library preparation using the TruMethyl WG method v.1.9 (Cambridge Epigenetix) as previously described (30). Features of retained and non-retained introns (length, GC content, CpG density and methylation status) were analysed as previously described (31). Intron-retaining transcripts were visualized using the Integrative Genomics Viewer (IGV), and the University of California, Santa Cruz (UCSC) Human Genome Browser tools (hg38 assembly) (32,33). The curated gene annotations from the Reference Sequence (RefSeq) database were chosen as the representative isoforms for all intron-retaining transcripts of interest (34).

To identify biological processes enriched in genes subject to differential IR, Gene Ontology (GO) enrichment analyses were performed using GOseq (35). IR gene subsets were used as input, and all measured genes in either THP-1 or primary cells were used as background. GO terms over-represented with a P-value < 0.05 were considered significant.

Nanopore MinION cDNA sequencing and Bioinformatics

Nanopore direct cDNA sequencing (SQK-DCS109) was performed using the flow cell R9.4 on the MinION machine (Oxford Nanopore Technologies) following the manufacturers' instructions with minor modifications. Briefly, first strand cDNA was made from 100 ng of poly-A-enriched RNA using the VN primer and SuperScript II (Invitrogen) at 42°C for 50 min. After removal of RNA by RNase Cocktail Enzyme Mix (Thermo Fisher), second strand cDNA was made using random hexamers (Invitrogen) and LongAmp Taq Master Mix (New England Biolabs), which was followed by the End-prep and Adapter ligation before subjecting the library to the flow cell. The base-calling algorithm Albacore 2.3.1 (Oxford Nanopore Technologies) was used to process the raw FAST5 files. About half a million reads that passed the default quality threshold were mapped to the human genome (hg38 assembly) using Minimap2 (36) with -ax splice and -k14 options. Alignments with MAPQ < 20 were skipped. SAM files were converted to the BAM format using samtools 1.9 and visualized in the UCSC genome browser (33). Further data processing and analysis was conducted using the R software (version 3.4.3).

Gene knockdown in THP-1 cells

To inhibit NMD, THP-1-derived macrophages were transfected with 300 nM *UPF1* siRNA (sense: 5′-GAUGCAGUUCCGCUCCAUUdTdT-3′, antisense: 5′-AAUGGAGCGGAACUGCAUCTdTdT-3′). To inhibit nuclear degradation by the RNA exosome, THP-1 macrophages were transfected with 300 nM *EXOSC10* siRNA (sense: 5′-GAAGGCAGCUGAGCAAACAdTdT-3′, antisense: 5′-UGUUUGCUCAGCUGCCUUCdTdT), or 300 nM *EXOSC11/DIS3* siRNA (sense: 5′-AGGUAGAGUUGUAGGAAUAdTdT-3′, antisense: 5′-UAUUCCUACAACUCUACCUdTdT). ON-TARGET*plus* non-targeting siRNA (GE Dharmacon) was used as a negative control. All transfections were performed using the Cell Nucleofector™ (Lonza) according to the manufacturers' instructions.

Nuclear and cytoplasmic isolation

Nuclear and cytoplasmic fractions were prepared from 5 × 10^6 THP-1 monocytes and THP-1-derived macrophages using the NE-PER™ Nuclear and Cytoplasmic Extraction Kit (Thermo Scientific) according to the manufacturers' instructions. Nuclear and cytoplasmic fractions were supplemented with 1% (v/v) Halt™ protease inhibitor (Thermo Scientific) and 0.2 U/μl RNase inhibitor (Sigma-Aldrich), to minimise protein and RNA degradation.

Proteomics sample preparation using SDB-RPS StageTips

Prior to lysis, cells on 10 cm tissue culture dishes were washed once in PBS at room temperature and then lysed by

addition of 1 ml of lysis buffer (4% sodium deoxycholate, 0.1 M Tris–HCl pH 8.0) and scraping the cells at room temperature. Lysates were immediately heated to 95°C for 10 min. Lysates were sonicated using a QSonica Q800R2 with 30 s on time, 30 s off time, for 10 min total sonication time using 20% amplitude at room temperature. Lysates were then clarified by centrifugation at 18 000 × g for 10 min at room temperature. The supernatants were retained and protein concentration determined by BCA assay (Thermo). Protein digestion and peptide clean-up was performed as described previously (37). Briefly, 20 μg protein lysate was made up to a total volume of 25 μl in SDC buffer (4% sodium deoxycholate, 10 mM TCEP, 40 mM chloroacetamide and 100 mM Tris–HCl pH 8.5) and heated to 95°C for 10 min to denature, reduce and alkylate proteins. Once cooled to room temperature and diluted 4-fold with 75 μl of water. Trypsin was added (from 1 mg/ml stock solution in 50 mM acetic acid) to digest proteins at 1:20 ratio (protease:protein, μg/μg) and digested at 37°C for 16 h. An equal volume (100 μl) of 99% ethylacetate/1% TFA was added to the digested peptides and vortexed. SDB-RPS StageTips were generated by punching double-stacked SDB-RPS discs (Sigma, Cat#66886-U) with an 18-gauge needle and mounted in 200 μl tips (Eppendorf). For clean-up utilising the Spin96, each tip was wetted with 100 μl of 100% acetonitrile and centrifuged at 1000 × g for 1 min. Following wetting, each StageTip was equilibrated with 100 μl of 0.1% TFA in H2O and 30% methanol/1% TFA with centrifugation for each at 1000 × g for 3 min. Each StageTip was then loaded with the equivalent of ∼20 μg peptide in 100 μl of the entire lower aqueous phase. The peptides were washed twice with 100 ul of 99% ethylacetate/1% TFA, which was followed by one wash with 100 μl of 0.2% TFA in water. To elute, 100 μl of 5% ammonium hydroxide/80% acetonitrile was added to each tip and centrifuged as above for 5 min into a unskirted PCR plate. Samples in the PCR plate were dried using a GeneVac EZ-2 using the ammonia setting at 35°C for 1 h. Dried peptides were resuspended in 60 μl of 5% formic acid and stored at 4°C until analysed by LC–MS.

Proteomics LC–MS/MS and analysis of spectra

Using a Thermo Fisher RSLCnano UHPLC, peptides in 5% (vol/vol) formic acid (injection volume 3 μl) were directly injected onto a 50 cm × 75 um C18 (Dr Maisch, Ammerbuch, Germany, 1.9 μm) fused silica analytical column with *a* ∼10 μm pulled tip, coupled online to a nanospray ESI source. Peptides were resolved over gradient from 5% acetonitrile to 40% acetonitrile over 140 min with a flow rate of 300 nl min^{-1}. Peptides were ionized by electrospray ionization at 2.3 kV. Tandem mass spectrometry analysis was carried out on a Fusion Lumos mass spectrometer (Thermo Fisher) using HCD fragmentation. The data-dependent acquisition method used acquired MS/MS spectra of the top 20 most abundant ions at any one point during the gradient. RAW data were analysed using the quantitative proteomics software MaxQuant (38) (version 1.6.3.4). Peptide and protein level identification were both set to a false discovery rate (FDR) of 1% using a target-decoy based strategy. The integrated MaxQuant Andromeda search engine (39) was used for peptide identification. The database supplied to the search engine for peptide identifications contained both the human UniProt database downloaded on 14th August 2018. Mass tolerance was set to 4.5 ppm for precursor ions and MS/MS mass tolerance was 20 ppm. Enzyme specificity was set to trypsin, with a maximum of 2 missed cleavages permitted. Deamidation of Asn and Gln, oxidation of Met, pyro-Glu and protein N-terminal acetylation were set as variable modifications. Carbamidomethyl on Cys was searched as a fixed modification. We used the MaxLFQ algorithm for label-free quantitation, integrated into the MaxQuant environment (38,40). The MaxQuant output was processed and analysed using R software (version 3.4.3) and plotted using Tableau (version 2019.2).

Western blotting

Protein lysates were loaded onto precast SDS-PAGE gels (Invitrogen) and subjected to electrophoresis before being transferred onto polyvinylidene difluoride (PVDF; Millipore) membranes. Membranes were blocked with 5% (w/v) skim milk for 1 h at room temperature and incubated overnight with a rabbit anti-UPF1 (1:1000, Cell Signalling #9435), a rabbit anti-EXOSC10 (1:800, Abcam ab50558), a rabbit anti-DIS3 (1:750, Sigma HPA039281) a rabbit anti-Lamin-B1 (1:2000, Abcam ab16048), or a mouse anti-GAPDH (1:2000, Abcam ab8245). Following washes, membranes were incubated with HRP-conjugated secondary anti-rabbit or anti-mouse antibody (1:5000; Chemicon AP182P or AP192P), and exposed using SuperSignal™ West Pico PLUS Chemiluminescent Substrate (Pierce) on a Bio-Rad ChemiDoc™ Imaging System (Bio-Rad).

ELISA

Human CXCL2 concentration in cell culture supernatants was detected using the Human CXCL2/GRO beta DuoSet ELISA (R&D Systems) according to the manufacturers' instructions. For measurement, Pierce™ 1-Step™ Ultra TMB-ELISA Substrate Solution (Thermo Scientific) was used, and absorbance was determined using a HT-Fret Tecan Infinite M1000 Pro (Tecan Group).

Statistical analysis

For statistical analyses of mRNA sequencing data processed by IRFinder (27) or DESeq2 (28), Benjamini–Hochberg-correction was used as a false discovery rate control, for *P*-values derived from an Audic and Claverie test (41) or Wald test, respectively, where adjusted $P < 0.05$ was considered significant. The overlap of IR events between donors were measured using Fisher's Exact test with significance denoted by $P < 0.05$. Data analysis for proteomics was performed using R and plotted using Tableau. Fold-changes for protein abundance were calculated using the mean in each group. Statistical significance for protein abundance changes between groups was calculated using a Student's t-test and the resulting *P*-values were adjusted to control for multiple testing using the Benjamini-Hochberg correction. Significance was set at $P < 0.05$. All other statistical analyses were performed using GraphPad Prism software, version 7.02 (GraphPad Software). Statistical signif-

icance was determined using an unpaired two-tailed Student's *t*-test or Mann-Whitney U test, where $P < 0.05$ was considered significant. All error bars shown represent either the standard error of the mean (SEM) or 1.5 times the interquartile range, from independent experiments.

RESULTS

Decreased intron retention is associated with an increase in the expression of genes important for monocyte-to-macrophage differentiation

The human monocytic leukaemia cell line, THP-1, is commonly used to derive macrophage-like cells via treatment with PMA *in vitro* (25). PMA treatment stimulates the expression of macrophage colony-stimulating factor (M-CSF), which is essential for macrophage maturation and function (22,42). Macrophage-like cells were robustly derived via treatment of THP-1 cells with PMA *in vitro* (Figure 1A–C). Consistent with previous reports (25,43,44), THP-1-derived macrophage-like cells demonstrated increased size, granularity and pseudopodia, and upregulated cell-surface molecules characteristic of terminally differentiated macrophages (Figure 1A–C).

We performed mRNA sequencing to curate differential IR events in undifferentiated THP-1 monocytic cells (Mo THP-1) and THP-1-derived macrophage-like cells (Mϕ THP-1). Using IRFinder (27), we identified 1126 differentially retained introns (adjusted $P < 0.05$, Audic and Claverie test) in 822 genes between the two cell types. A higher degree of IR was observed in Mo THP-1 ($n = 881$) compared to Mϕ THP-1 ($n = 245$), indicating that IR generally decreases during monocyte-to-macrophage differentiation *in vitro* (Figure 1D).

Consistent with previous reports (3,5,11,31), retained introns in Mo and Mϕ THP-1 cells were found to be significantly shorter in length, and higher in GC content and CpG density compared to non-retained introns (Supplementary Figure S1A-C). We also observed substantially reduced levels of CpG methylation in retained introns when compared to non-retained introns in both cell types (Supplementary Figure S1D), consistent with our previous observations in granulocytes and other cell types (31). By performing Nanopore sequencing, we observed different patterns of gene-specific IR events; some genes showed retention of single introns within entire transcripts while others showed retention of multiple introns within single transcripts (Supplementary Figure S2). Decreased global IR in Mϕ THP-1 cells was more likely to be associated with increased spliced transcript expression; of the genes displaying decreased IR, 56% (350/625) increased in spliced transcript expression (Figure 1E). Conversely, increased IR coincided with decreased spliced transcript expression in 60% (119/197) of genes (Figure 1F). Using mass spectrometry, we confirmed an increase in overall protein levels in 63% (59/94) proteins derived from genes exhibiting decreased IR and increased spliced transcript expression (FDR < 0.05, Figure 1G, Supplementary Table S2). For proteins derived from genes showing increased IR and reduced spliced transcript expression, 53% (33/62) proteins were also significantly reduced (FDR < 0.05, Figure 1G, Supplementary Table S2).

To determine functional associations of intron-retaining transcripts showing an inverse relationship between IR and spliced transcript expression, GO enrichment analyses were performed. Genes with reduced IR and increased expression in Mϕ THP-1 macrophages are overrepresented in pathways associated with the regulation of interferon and cytokine-mediated signalling as well as macrophage-related functions, including vesicle-mediated transport, secretion of lysosomal enzymes and autophagy (Figure 1H). In contrast, genes demonstrating increased IR and decreased spliced transcript expression were particularly enriched for RNA splicing, processing and localisation functions (Figure 1I). These results indicate that distinct groups of intron-retaining transcripts, showing differential IR and altered spliced transcript expression, were separately clustered in processes relevant to macrophage function and development.

Intron retention is associated with changes in the expression of specific splicing factors during macrophage differentiation

Since IR predominantly decreased in Mϕ compared to Mo THP-1 cells, we hypothesise that this observation is associated with an increase in the expression of splicing factors that may contribute to more efficient splicing in Mϕ cells. Surprisingly, both mRNA-seq and mass spectrometry data indicate a decrease in the expression of >50% splicing factors that we assessed in Mϕ compared to Mo THP-1 cells (Supplementary Figure S3A and B). Only four splicing factors showed a significant increase in their expression (adjusted $P < 0.05$, Wald test, Supplementary Figure S3A), including QK1 that has previously been demonstrated to promote splicing during monocyte-to-macrophage differentiation (45). However, a significant increase was not observed at the protein level; presumably due to the lower abundance of this protein in macrophages that limits the consistency of detecting it by mass spectrometry. HNRNPH2 is the only splicing factor with increased levels in Mϕ compared to Mo THP-1 cells using mass spectrometry. Collectively, our data indicate that IR changes may be linked to altered expression of specific splicing factors rather than a global increase in splicing factor expression.

Specific intron retention events affect key genes involved in macrophage development and function

Using RT-qPCR, we validated differential IR between Mo and Mϕ THP-1 cells in 11/13 (85%) selected mRNA transcripts. We confirmed that decreased and increased IR was inversely correlated with the expression of the spliced gene (Figure 2A and B, and Supplementary Figure S4A and S4B). In most cases, the fold-change in IR levels was less than the fold-change in spliced transcript expression indicating that a proportion of intron-retaining transcripts may be degraded and not measurable by RT-qPCR. Among the intron-retaining transcripts tested was *ID2*, a negative transcriptional regulator known to be important in myeloid development, including monocyte-to-macrophage differentiation (46). The other intron-retaining transcripts validated by RT-qPCR, *IRF7*, *TYMP*, *ENG* and *LAT*, have also been shown to be highly expressed in macrophages,

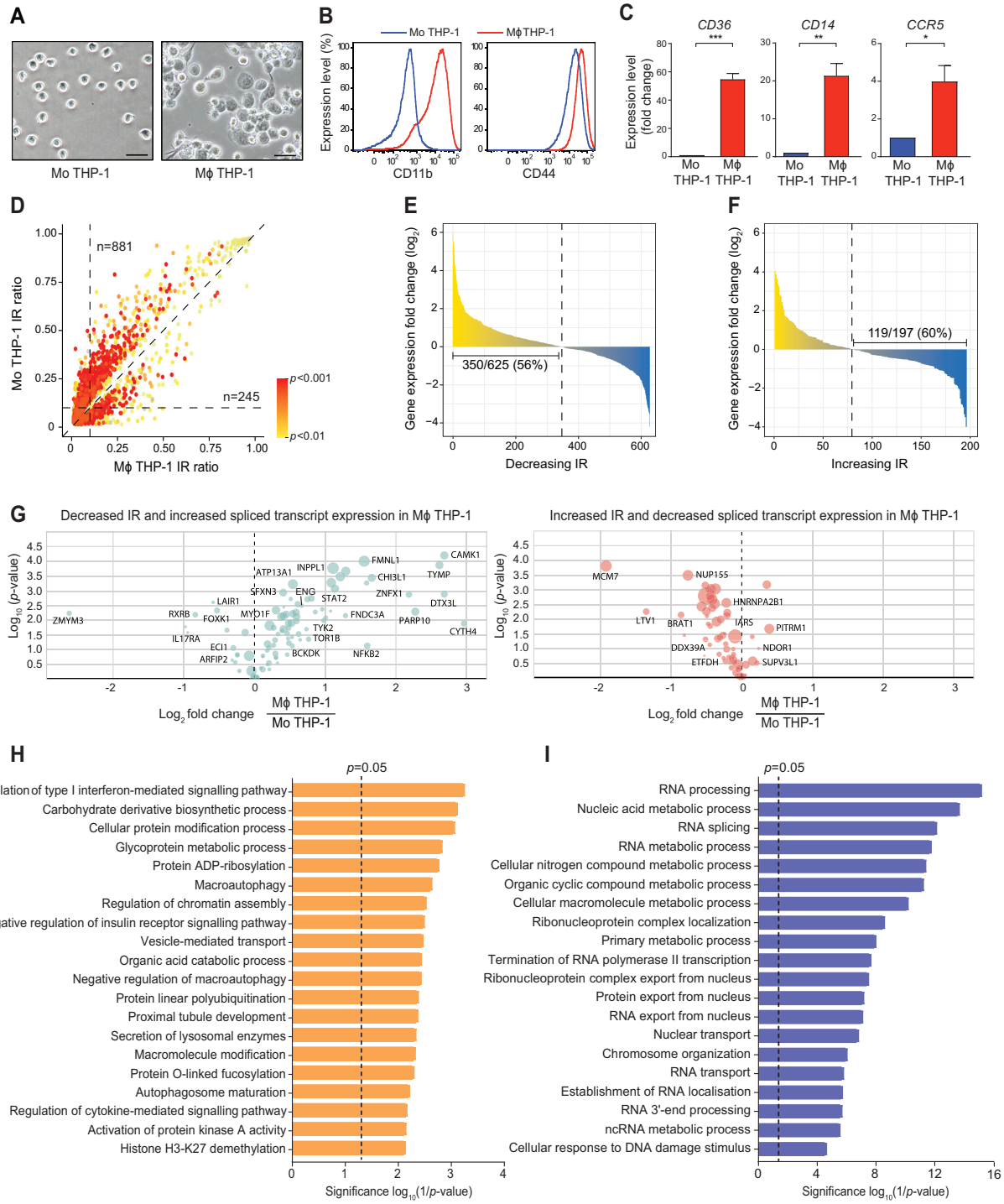

Figure 1. Decreased intron retention is associated with an upregulation of genes important for monocyte-to-macrophage differentiation. (**A**) Phase contrast microscopy images confirming morphological changes between THP-1 monocytic cells (Mo THP-1) and THP-1-derived macrophages (Mϕ THP-1). Scale bar, 50 μm. (**B**) Flow cytometry profiles showing the relative expression of cell surface markers CD11b and CD44 known to be enriched in macrophages. Blue and red lines represent Mo THP-1 cells and Mϕ THP-1 macrophages respectively. (**C**) Expression of *CD36*, *CD14* and *CCR5* transcripts in Mϕ THP-1 macrophages compared to Mo THP-1 cells (normalised to *B2M* expression) measured by RT-qPCR. (**D**) Scatterplot showing the distribution of significantly retained introns (adjusted $P < 0.05$, Audic and Claverie test) in either Mo or Mϕ THP-1 cells. 1126 differential IR events, with an IR ratio $\geq$ 0.1 in one cell type (dashed horizontal/vertical lines), affecting 822 genes, were considered for further analyses. (**E** and **F**) Waterfall plots showing RNA expression fold change for genes with decreasing IR ($n = 625$) and increasing IR ($n = 197$). Vertical dashed lines indicate the inflection points. (**G**) Volcano plots showing protein-level abundance changes from proteomic analysis, where each point represents one protein. The y-axis shows the -Log_{10} (*P*-value) from a Benjamini-Hochberg corrected Student's *t*-test for each protein. (**H** and **I**) Bar graphs showing significantly overrepresented functional categories ($P < 0.05$) determined by gene ontology analysis of genes with reduced and increased IR in Mϕ THP-1 compared to Mo THP-1. All data, unless otherwise specified, are from three independent experiments, each in triplicate, and show mean ± SEM. An unpaired two-tailed Student's *t*-test was used to determine significance, denoted by * ($P < 0.05$), ** ($P < 0.01$) and *** ($P < 0.001$).

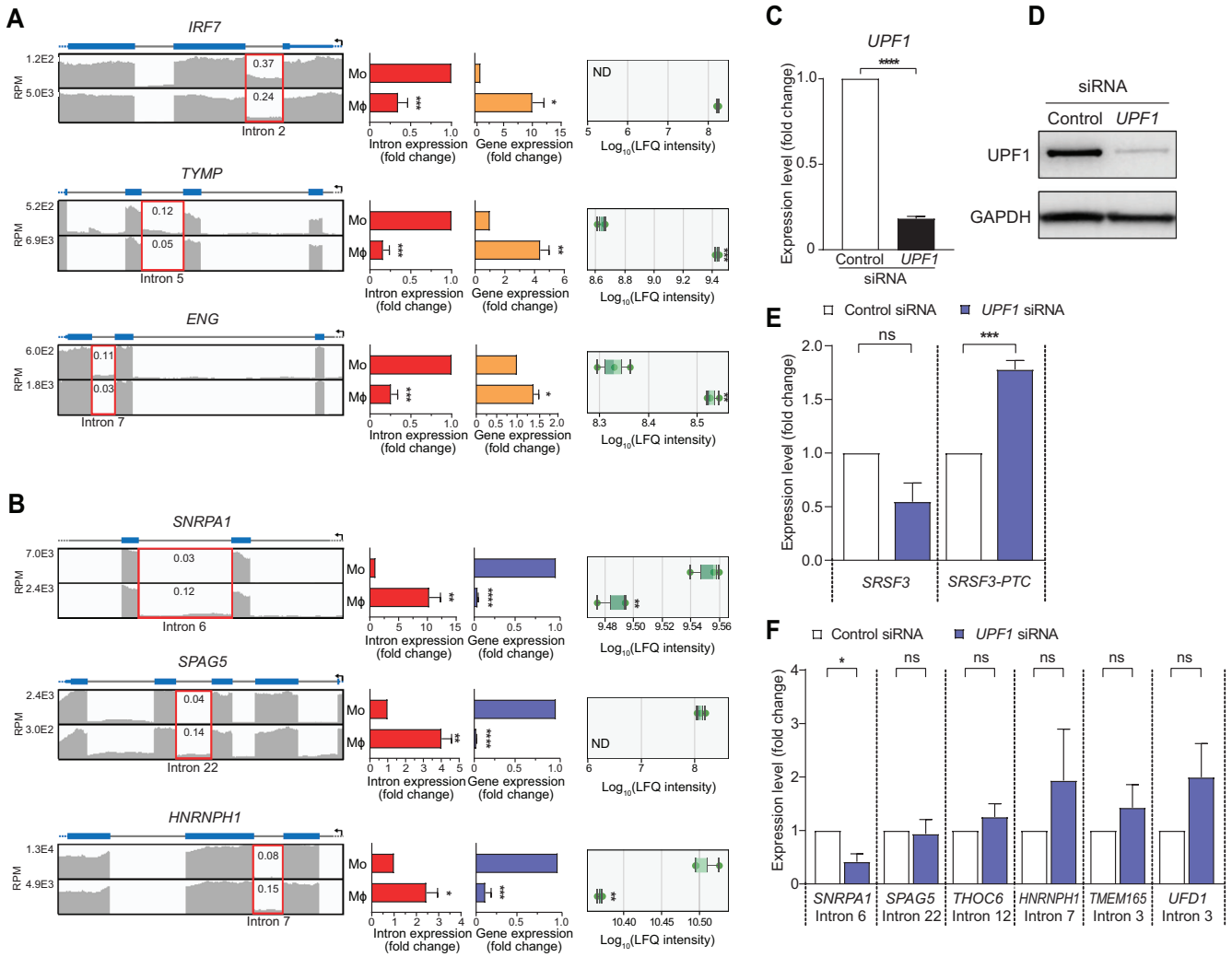

Figure 2. Specific intron retention events are associated with differential expression of key genes involved in monocyte-to-macrophage differentiation. Coverage plots of mRNA sequencing reads are shown for genes with decreased IR and increased mRNA expression (**A**), and increased IR and decreased mRNA expression (**B**). Coverage plots of reads per million mapped reads (RPM) in THP-1 monocytic cells (Mo) and THP-1-derived macrophages (Mϕ) are shown on separate linear scales. Translational direction (black arrow), exons (blue boxes), 5′ and 3′ UTRs (thinner blue boxes), and introns (horizontal grey lines) are shown above. IR ratios of introns of interest (highlighted by red boxes) are shown. Bar graphs on the right show expression fold change of retained introns in Mϕ, compared to Mo by RT-qPCR. Intronic expression is normalised to the expression of transcripts that span flanking exons. Expression of spliced transcripts (orange or blue bars) are normalised to *B2M* expression. Box and whisker plots on the right show protein abundance of corresponding IR-affected genes in Mo and Mϕ, as measured by proteomic analysis. (**C**) Fold change of *UPF1* transcript expression in Mϕ cells transfected with *UPF1* siRNA, compared to Mϕ cells transfected with non-targeting control siRNA by RT-qPCR. (**D**) Western blot showing UPF1 protein levels in Mϕ cells transfected with *UPF1* siRNA and non-targeting control siRNA. GAPDH was used as a loading control. (**E**) RT-qPCR analysis of *SRSF3* and PTC-containing *SRSF3* expression in Mϕ cells transfected with *UPF1* siRNA, compared to cells transfected with non-targeting control siRNA. (**F**) Expression of intron retaining transcripts in Mϕ macrophages transfected with *UPF1* siRNA, compared to non-targeting control siRNA-transfected cells by RT-qPCR. Intronic expression is normalised to the expression of transcripts that span flanking exons. All data are from three independent experiments, each in triplicate, and show mean ± SEM. An unpaired two-tailed Student's *t*-test was used to determine significance, denoted by * ($P < 0.05$), ** ($P < 0.01$), *** ($P < 0.001$), **** ($P < 0.0001$) and ns (not significant).

and play roles in tissue infiltration, adhesion, phagocytosis and inflammatory signalling (47–52) (Figure 2A and Supplementary Figure S4A). Furthermore, transcripts showing increased IR and decreased spliced transcript expression were found to be transcribed from genes involved in RNA splicing and processing (*SNRPA1*, *HNRNPH1* and *THOC6*) (6,53,54) (Figure 2B and Supplementary Figure S4B). Notably, spliced transcript expression changes associated with IR changes were also reflected at the protein levels for 72% (8/11) candidates, as measured using mass spectrometry (Figure 2A and B, and Supplementary Figure S4B. These results correspond to our GO enrichment analyses and indicate that dynamic changes in IR affect important macrophage-related genes and proteins.

Intron-retaining transcripts are detained in the nucleus

To determine whether intron-retaining transcripts were subject to cytoplasmic NMD during monocyte-to-macrophage differentiation, we knocked down the core NMD factor

UPF1 in THP-1-derived macrophages (Figure 2C and D) (11,14). We confirmed NMD inhibition by detecting significantly increased levels of *SRSF3* transcripts with a PTC-containing poison exon, which are known to be subject to NMD (Figure 2E) (55). The level of IR detected in intron-retaining transcripts *SNRPA1*, *SPAG5*, *THOC6*, *HNRNPH1*, *TMEM165*, *UFD1* did not significantly increase following UPF1 knockdown, indicating they are not subject to NMD (Figure 2F).

Intron-retaining transcripts may be protected from cytoplasmic NMD because they are detained in the nucleus (7,8,12,15). Using nuclear and cytoplasmic fractionation, we aimed to establish the localisation of intron-retaining transcripts in Mo and Mϕ THP-1 cells. The purity of cellular fractions was assessed by western blot and RT-qPCR. The nuclear marker Lamin-B1 was significantly enriched in the nuclear fractions of both cell types, and GAPDH was only detected in the cytoplasmic fractions (Figure 3A). Similarly, *MALAT1*, a polyadenylated non-coding RNA known to be detained in the nucleus (56), was significantly enriched in the nuclear fractions, while mature *B2M* transcripts were enriched in cytoplasmic fractions (Figure 3B and C). RT-qPCR was then repeated for the four intron-retaining transcripts with the highest levels of IR in each cell type, to compare their enrichment between the nuclear and cytoplasmic isolates. We found all intron-retaining transcripts except for *TYMP* were 9- to 150-fold enriched in the nuclear fraction of Mo THP-1 cells (Figure 3D). In THP-1 macrophages, all intron-retaining transcripts examined were enriched (11- to 100-fold) in the nuclear fraction compared to the cytoplasmic fraction (Figure 3E). These results indicate that functionally relevant, intron-retaining transcripts are detained in the nuclei of monocytes and macrophages, which explains their protection from NMD.

After establishing the localisation of intron-retaining transcripts with decreased transcript expression in the nuclei of THP-1 macrophages, we aimed to determine whether these transcripts were subject to RNA exosome-mediated degradation in the nucleus. We confirmed that *EXOSC10*, an important catalytic component of the nuclear exosome complex (12,19,57), is primarily localised in the nuclei of THP-1 macrophages (Supplementary Figure S5A). We subsequently knocked-down *EXOSC10* expression in these cells (Figure 4A and B), and confirmed that EXOSC10 activity was inhibited by detecting significantly increased levels of PROMPTs known to be subject to RNA exosome-mediated degradation (Figure 4C) (58). mRNA sequencing and IRFinder analysis (27) of control and *EXOSC10*-knockdown cells revealed modest changes in IR levels, suggesting intron-retaining transcripts are not primarily regulated by exosome-mediated degradation (Figure 4D). This result was further supported by RT-qPCR analysis of the nuclear-detained, intron-retaining transcripts *SNRPA1*, *SPAG5* and *HNRNPH1*, which showed no significant increase in IR levels following *EXOSC10* knockdown (Supplementary Figure S5B). These observations were recapitulated following knockdown of *EXOSC11*/*DIS3*, another important catalytic subunit of the nuclear exosome complex (12,19,59), (Supplementary Figure S5C and S5D). After confirming that DIS3 activity was inhibited by detecting significantly increased levels of RNAs known to be subject to DIS3-mediated degradation (Supplementary Figure S5E) (59), we similarly did not observe significant increases in IR levels in the transcripts of interest (Supplementary Figure S5F). Overall, these results indicate that nuclear-detained, intron-retaining transcripts are insensitive to both NMD and RNA exosome-mediated degradation in monocytes and macrophages.

Substantially decreased intron retention is a conserved phenomenon in cell line and primary human monocyte-to-macrophage differentiation

To validate our findings in primary cells, we first compared previously published primary monocyte and macrophage mRNA sequencing data (29) using IRFinder (27). In these experiments, monocytes derived from four healthy donors (Donors L1, L2, L3 and L4) were differentiated *in vitro* using M-CSF over 7 days (29). We found higher levels of IR in primary monocytes compared to M-CSF-derived macrophages in all donor samples (Figure 5A, Supplementary Figure S6A–C). For example, 826 introns in 585 genes showed significant differential retention (adjusted $P < 0.05$, Audic and Claverie test) between the two cell types in Donor L1 (Figure 5A). Of these introns, 96% (796/826) were increased in monocytes, indicating that IR is substantially decreased during *in vitro* differentiation of primary human monocytes into macrophages.

We also found significant overlap between IR events in monocytes (odds ratio 14.1; $P = 2.5E{-}184$, Fisher's Exact Test) and macrophages (odds ratio 15.9; $P = 5.9E{-}53$, Fisher's Exact Test) derived from the four donors (Supplementary Figure S6D). Downregulated IR events during primary monocyte-to-macrophage differentiation were also common between donors (odds ratio of 10.4; $P = 9.9E{-}79$, Fisher's Exact Test) (Supplementary Figure S6D). For further analyses, we pooled genes subject to decreased IR from each donor. The IR-affected genes which showed decreased IR and increased spliced transcript expression (52%, 645/1245) displayed a greater skew in spliced transcript expression fold change (Figure 5B). GO analysis of these genes revealed significant representation of pathways associated with leukocyte-mediated activation, immune response, as well as macrophage-related functions such as vesicle-mediated transport and membrane/lamellipodium remodelling (Figure 5C).

These findings from primary cells recapitulate our observations in THP-1 cells, indicating that the changes in IR are likely an important and conserved regulatory mechanism of gene expression control in human monocyte and macrophage biology.

The intron retention program continues to undergo dynamic changes during macrophage activation

We further investigated the role of IR during macrophage activation. After their differentiation with PMA, THP-1-derived Mϕ-like macrophages can be further polarised to an M1-like phenotype following treatment with LPS and IFN-γ (23,60). M1-like THP-1 macrophages were robustly derived via treatment of Mϕ THP-1 cells with LPS and IFN-γ for 6 hours *in vitro* (Figure 6A and B). Consis-

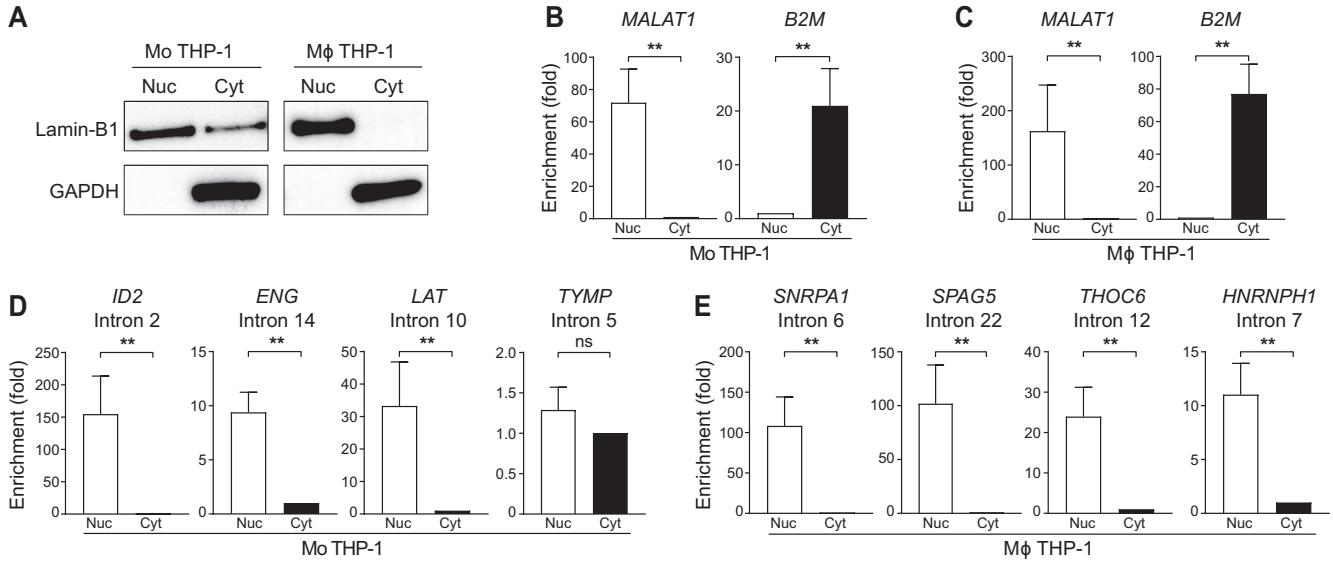

Figure 3. Intron-retaining transcripts are detained in the nuclei of THP-1 monocytic cells and macrophages. (**A**) Western blot comparing levels of Lamin B1 (nuclear marker) and GAPDH (cytoplasmic marker) in cell-equivalent fractions of nuclear and cytoplasmic protein from THP-1 monocytes (Mo) and THP-1-derived macrophages (Mϕ). (**B** and **C**) RT-qPCR analyses of *MALAT1* and *B2M* transcript fold enrichment in nuclear and cytoplasmic cell-equivalent fractions of RNA from Mo and Mϕ cells. (**D** and **E**) Fold enrichment of intron-retaining transcripts in cell-equivalent fractions of nuclear and cytoplasmic RNA from Mo and Mϕ cells by RT-qPCR. All data are from six independent experiments, each in triplicate, and show mean ± SEM. A two-tailed Mann–Whitney *U*-test was used to determine significance, denoted by ** ($P < 0.01$) and ns (not significant). Nuc, nucleus; Cyt, cytoplasm.

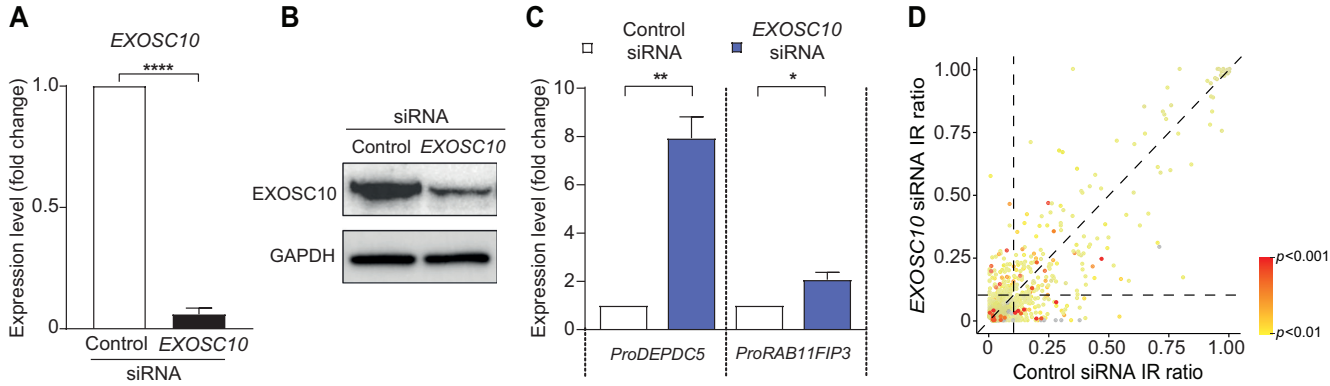

Figure 4. Nuclear-detained intron-retaining transcripts are insensitive to RNA exosome-mediated degradation. (**A**) Fold change of *EXOSC10* transcript expression in THP-1-derived macrophages (Mϕ) transfected with *EXOSC10* siRNA, compared to non-targeting control siRNA-transfected cells by RT-qPCR (normalised to *B2M* expression). (**B**) Western blot showing EXOSC10 protein levels in Mϕ-like THP-1 macrophages transfected with *EXOSC10* siRNA and non-targeting control siRNA. GAPDH was used as a loading control. (**C**) RT-qPCR analysis of PROMPT (*ProDEPDC5* and *ProRAB11FIP3*) expression in Mϕ-like THP-1 macrophages transfected with *EXOSC10* siRNA, compared to non-targeting control siRNA-transfected cells. (**D**) Scatterplot showing the distribution of significantly differentially retained introns (adjusted $P < 0.05$, Audic and Claverie test) in *EXOSC10* siRNA-transfected and non-targeting control siRNA-transfected Mϕ cells. 84 differential IR events, with an IR ratio ≥0.1 in one condition (dashed horizontal/vertical lines), affecting 80 genes, were considered for further analyses. All data are from three independent experiments, each in triplicate, and show mean ± SEM. An unpaired two-tailed Student's *t*-test was used to determine significance, denoted by * ($P < 0.05$), ** ($P < 0.01$), **** ($P < 0.0001$).

tent with previous reports (23,61,62), M1-polarised THP-1 macrophages demonstrated cell-surface and molecular markers characteristic of activated, proinflammatory M1 macrophages (Figure 6A and B).

Using IRFinder (27), we analysed mRNA sequencing data from THP-1-derived Mϕ- and M1-like macrophages to determine differential IR levels. We identified 768 differentially retained introns (adjusted $P < 0.05$, Audic and Claverie test) in 578 genes between the two cell types. We observed roughly similar degrees of both increased (n = 442) and decreased (n = 326) IR events in M1-like macrophages (Figure 6C).

We also compared the primary Mϕ- and M1-like macrophage mRNA sequencing data retrieved from Liu *et al.* using IRFinder (27). In these experiments, monocytes derived from four healthy donors were differentiated *in vitro* using GM-CSF over 7 days, then polarised to an M1-like phenotype using LPS and IFN-γ over 8 h (29). For all individuals, less differential IR was observed when compared to our previous observations made in THP-1 cells (Figure

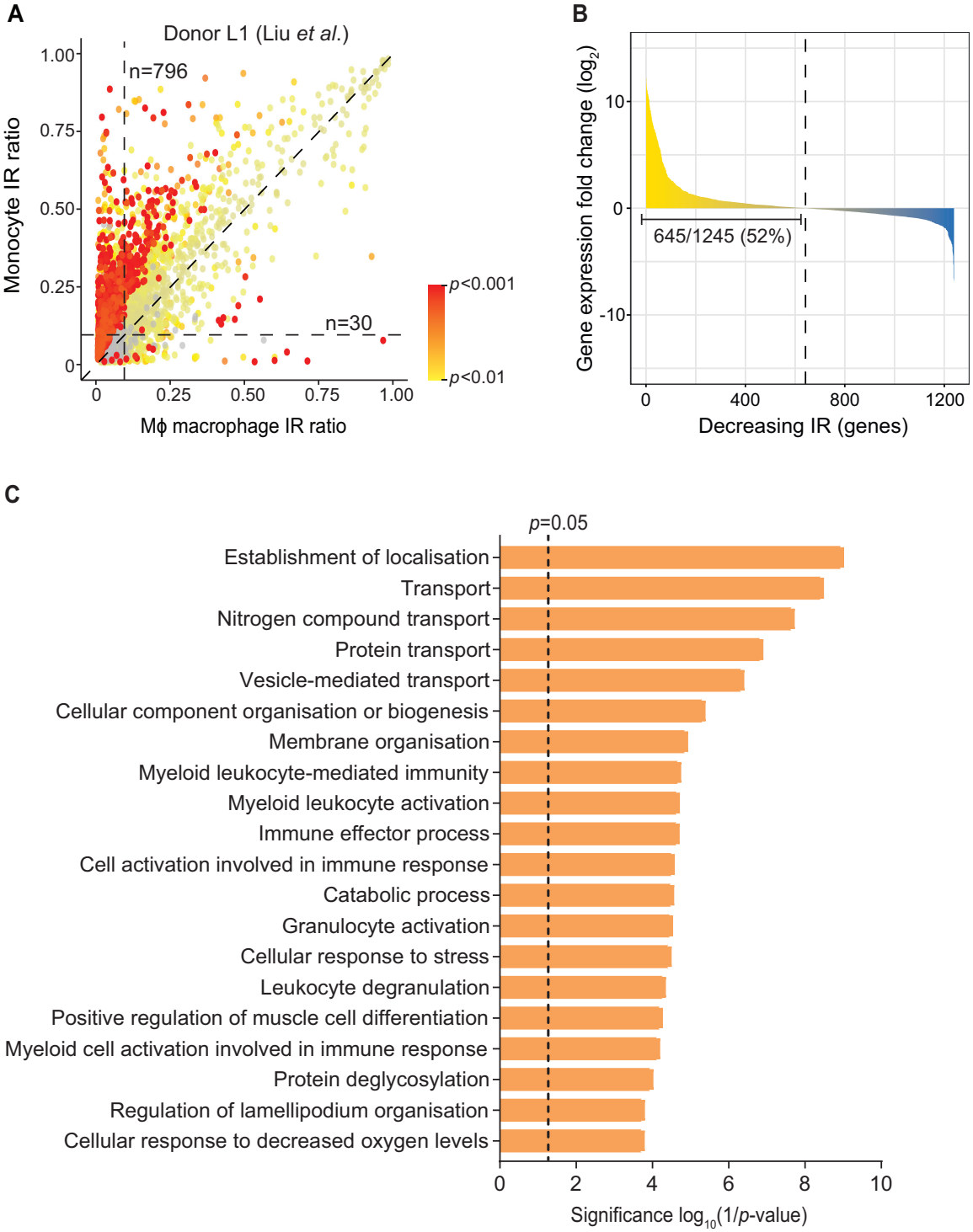

Figure 5. Intron retention substantially decreases during primary monocyte-to-macrophage differentiation. (**A**) Scatterplot showing the distribution of significantly differentially retained introns (adjusted $P < 0.05$, Audic and Claverie test) in primary monocytes and Mϕ macrophages derived from Donor L1 (Liu *et al.*, 2018). 826 differential IR events, with an IR ratio ≥ 0.1 in one cell type (dashed horizontal/vertical lines), affecting 585 genes, were considered for further analyses. (**B**) Waterfall plots showing transcript expression fold change for pooled genes with decreasing IR from all donors ($n = 1245$) (Liu *et al.*, 2018). (**C**) Bar graphs showing significantly overrepresented functional categories ($P < 0.05$) determined by gene ontology analysis of genes with reduced IR.

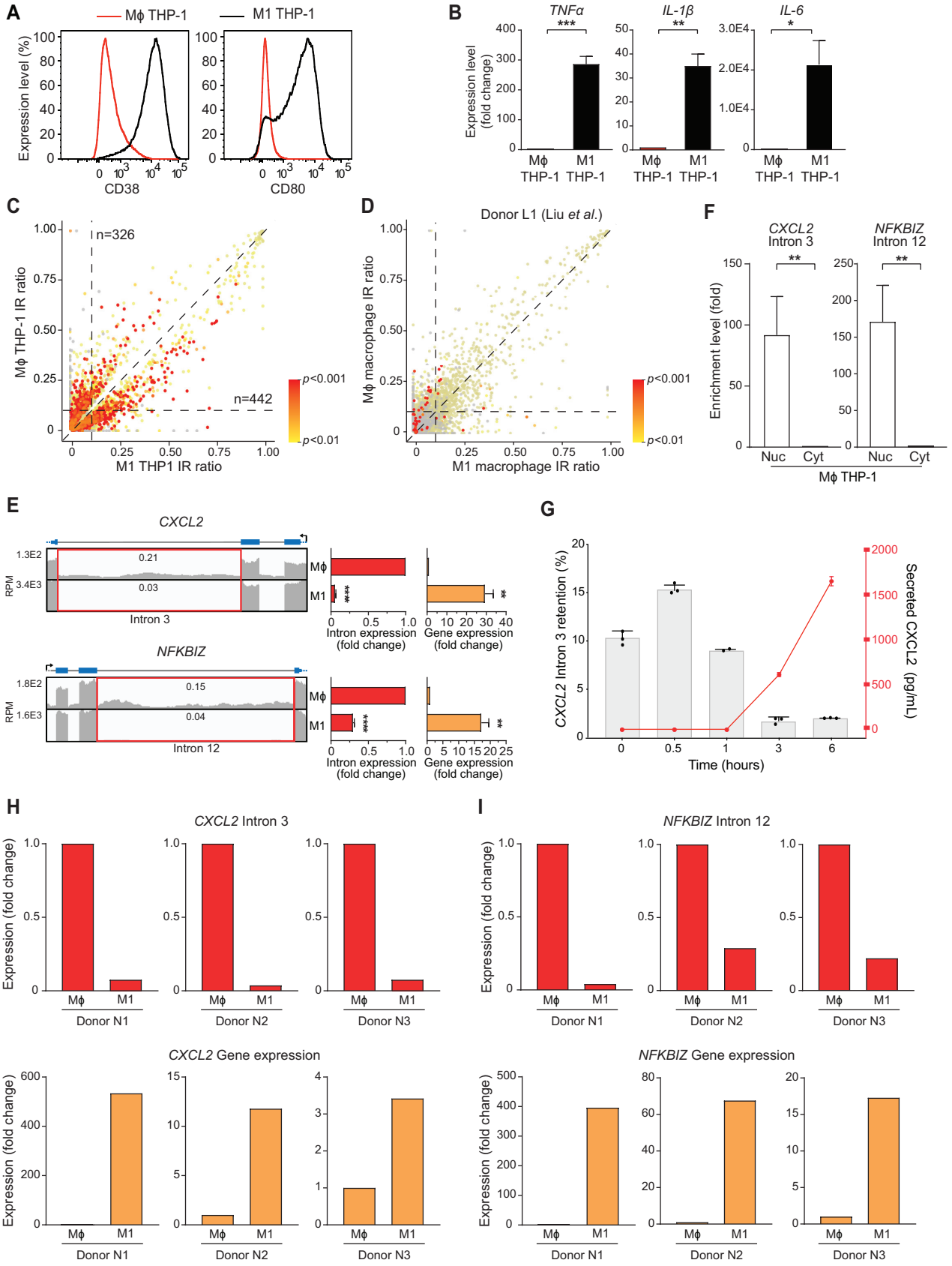

Figure 6. Transcripts encoding key proinflammatory regulators decrease in intron retention and increase in spliced transcript expression during macrophage activation. (**A**) Flow cytometry profiles showing the relative expression of M1-macrophage markers CD38 and CD80. Red line represents

6D and Supplementary Figure S7A–C). Between individuals, the overall direction in which IR levels changed during M1 macrophage activation was variable. For example, macrophages derived from Donor L1 exhibited significantly increased IR prior to activation (Figure 6D), whereas those derived from Donor L3 showed significantly increased IR following activation (Supplementary Figure S7B).

From these data, we conclude that IR is implicated in macrophage activation status, but the affected genes and IR pattern vary between different individuals, which may be attributed to genetic and/or environmental regulation.

Proinflammatory genes *CXCL2* and *NFKBIZ* are regulated by intron retention coupled with nuclear detention during macrophage activation

Despite a lack of an identifiable global pattern of IR changes, we identified *CXCL2* and *NFKBIZ* as key proinflammatory transcripts that are affected by IR during polarisation of THP-1-derived macrophage to an M1-like phenotype. Both *CXCL2* and *NFKBIZ* are known to be induced by bacterial antigens and are considered characteristic of M1-macrophage activation (63,64). When macrophages sense microbial infections, they secrete CXCL2, a potent neutrophil chemoattractant. This facilitates the recruitment of neutrophils to sites of infection, thereby limiting bacterial spread and promoting pathogen clearance (63). Similarly, NFKBIZ is produced by activated macrophages and acts as a transcriptional coactivator for proinflammatory cytokines IL-6 and IL-12, as well as CCL2, an important chemokine for monocyte recruitment during inflammation (64). Using RT-qPCR, we validated differential IR and spliced transcript expression of these genes. For both, we confirmed a significant decrease in IR coinciding with a robust upregulation in spliced transcript expression (Figure 6E).

To determine whether intron-retaining *CXCL2* and *NFKBIZ* transcripts were detained in the nuclei of macrophages prior to activation, we performed RT-qPCR on nuclear and cytoplasmic isolates from THP-1-derived Mϕ macrophages. We found significant levels of enrichment for both transcripts in the nuclear fractions (>90-fold) (Figure 6F). This indicates that mature, intron-retaining *CXCL2* and *NFKBIZ* mRNAs are detained in the nuclei of resting macrophages.

To demonstrate that a progressive decrease in intron-retaining transcripts resulted in a reciprocal increase in the production of protein, we measured the levels of *CXCL2* IR alongside secreted CXCL2 in a time-course experiment wherein Mϕ THP-1 cells were polarised with LPS and IFN-γ. Notably, intron-retaining *CXCL2* accumulation peaked half an hour following proinflammatory stimulation, then rapidly decreased the following 2.5 h, concomitant with a marked increase in CXCL2 secretion at 3 h (Figure 6G). The levels of *CXCL2* IR remained low as secreted CXCL2 was continuously detected at 6 h post polarisation. These results indicate that timely splicing of accumulated intron-retaining transcripts encoding a key macrophage chemotaxis factor was directly associated with its production and secretion.

We then compared the IR levels of *CXCL2* in the primary Mϕ-like macrophage and M1-like macrophages in previously reported mRNA sequencing data (29). Using IGV (32), we observed a similar decrease in IR of these genes during macrophage activation in all four donors (Supplementary Figure S7D). We then validated differential IR and spliced transcript expression of *CXCL2* and *NFKBIZ* in primary human macrophages polarised to an M1-like phenotype generated in our laboratory. In M1-like macrophages from three healthy donors (Supplementary Figure S7E), we confirmed significant decreases in *CXCL2* and *NFKBIZ* IR alongside significant increases in spliced transcript expression during M1-macrophage activation in each sample (Figure 6H and I). These findings demonstrate that nuclear detention of IR transcripts is an important mechanism regulating expression of these two important inflammatory genes.

DISCUSSION

The role of IR during monocyte-to-macrophage differentiation and M1-macrophage activation has not previously been elucidated. We used the THP-1 cell line as a model of monocyte-to-macrophage differentiation and macrophage activation to determine changes in IR and its impact on gene expression control during these processes. We then

←

THP-1-derived macrophages (Mϕ) and black line represents LPS and IFN-γ-polarised THP-1-derived macrophages (M1). (**B**) Expression of *TNFα*, *IL-1β* and *IL-6* transcripts in M1, compared to Mϕ cells (normalised to *B2M* expression). (**C**) Scatterplot showing the distribution of significantly retained introns (adjusted $P < 0.05$, Audic and Claverie test) in either Mϕ or M1 THP-1 cells. 768 differential IR events, with an IR ratio ≥0.1 in one cell type (dashed horizontal/vertical lines), affecting 578 genes, were considered for further analyses. (**D**) Scatterplot showing the distribution of significantly differentially retained introns (adjusted $P < 0.05$, Audic and Claverie test) in primary Mϕ and M1 macrophages derived from Donor L1 (Liu *et al.*, 2018). Thirty seven differential IR events, with an IR ratio ≥0.1 in one cell type (dashed horizontal/vertical lines), affecting 28 genes, were considered for further analyses. (**E**) Coverage plots of reads per million mapped reads (RPM) in Mϕ- and M1-like THP-1 macrophages are shown on separate linear scales for *CXCL2* and *NFKBIZ* genes. Translational direction (black arrow), exons (blue boxes), 5′ and 3′ UTRs (thinner blue boxes), and introns (horizontal grey lines) are shown above. IR ratios of introns of interest (highlighted by red boxes) are shown. Bar graphs on the right show expression fold change of retained introns in M1 compared to Mϕ cells by RT-qPCR analysis (normalised to the expression of the spliced product of its flanking exons). Expression of spliced transcript (orange bars) is normalised to *B2M* expression. (**F**) Fold enrichment of intron-retaining *CXCL2* and *NFKBIZ* in nuclear and cytoplasmic fractions from THP-1-derived Mϕ macrophages measured using RT-qPCR. Cell equivalent fractions of nuclear and cytoplasmic RNA are used in this analysis. Data are from six independent experiments, each in triplicate, and show mean ± SEM. A two-tailed Mann Whitney U-test was used to determine significance, denoted by ** ($P < 0.01$). (**G**) Percentage level of IR in *CXCL2* (bar graph) and amount of CXCL2 protein secreted over time (line graph), following proinflammatory stimulation of Mϕ macrophages, as measured by RT-qPCR and ELISA, respectively. (**H** and **I**) Expression of intron-retaining *CXCL2* or *NFKBIZ* (red bars) in primary M1 macrophages compared to primary Mϕ macrophages (normalised to the expression of the spliced product of its flanking exons). Expression of corresponding spliced transcripts (orange bars) are normalised to *B2M* expression. All data, unless otherwise specified, are from three independent experiments, each in triplicate, and show mean ± SEM. An unpaired two-tailed Student's *t*-test was used to determine significance, denoted by * ($P < 0.05$), ** ($P < 0.01$), *** ($P < 0.001$) and **** ($P < 0.0001$).

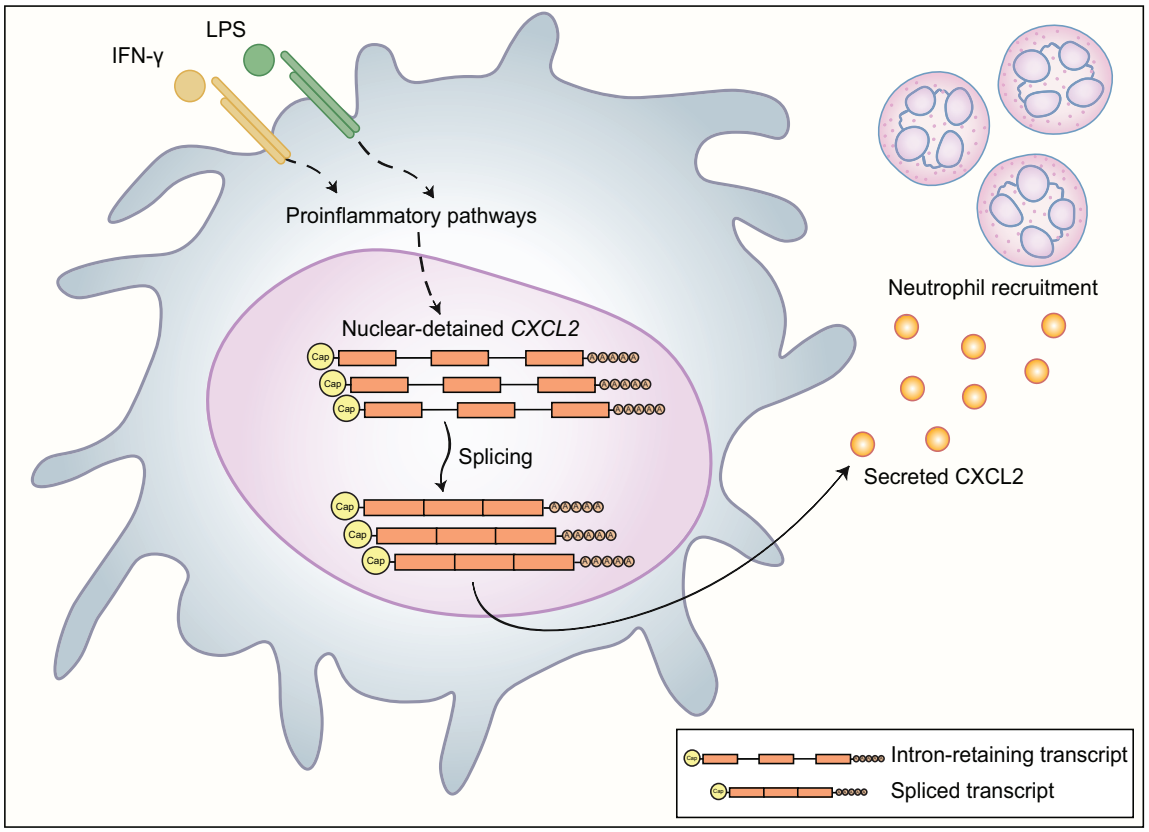

Figure 7. Working model showing intron retention coupled with nuclear detention regulates the expression of proinflammatory genes during the innate immune response. Before and during proinflammatory stimulation, macrophages store intron-retaining transcripts of proinflammatory response genes, including *CXCL2*, in the nucleus. Following accumulation, M1-polarised macrophages are well-poised for timely splicing of intron-retaining *CXCL2* transcripts to facilitate a burst of CXCL2 protein synthesis faster than *de novo* transcription and translation.

validated our findings in primary human cells. IRFinder (27) analyses of undifferentiated and THP-1-derived Mϕ-like cells revealed two separate clusters of introns subject to differential IR, with most introns decreasing in retention levels. Consistent with previous reports (3,4,11,31), intron-retaining transcripts in monocytes and macrophages exhibit conserved genetic and epigenetic features (Supplementary Figure S1). The detection of single full-length polyadenylated transcripts using Nanopore indicates that retention of some introns may be cooperatively regulated (Supplementary Figure S2). Our finding is consistent with the concept of 'all or none' splicing, reported previously in individual nascent RNA transcripts (65). Specifically, it has been shown that, when splicing of an intron occurs, it will rapidly promote the splicing of subsequent introns (66). Alternatively, fully unspliced transcripts may be removed more rapidly than partially spliced transcripts. Based on this concept, the retention of all introns in select transcripts may be indicative of an energy-efficient means to promote or repress gene expression.

We established that decreased IR is a conserved phenomenon during both human cell line and primary monocyte-to-macrophage differentiation. Although the limited sensitivity of LC-MS/MS constrained our analysis to only 258 proteins that were detected at significantly different levels between monocytes and macrophages, we observed an inverse correlation between IR and splice transcript expression/protein levels for approximately three-fifths of IR candidates that have corresponding proteomics data. Notably, the limitation of LC-MS/MS prevents detection of low molecular weight and/or secreted proteins derived from several IR candidates relevant to monocytes/macrophages including *ID2*, *LAT* and *UFD1*. Our GO analyses of the major gene cluster exhibiting decreased IR and upregulated splice transcript expression showed significant representation of immunoregulatory and macrophage-related functions in our cell line and pooled primary cell datasets from Liu *et al.*, 2018 (29). Similar to what has been strongly implicated in a variety of cell types (5,7–9), macrophages exhibit global reductions in IR in upregulated gene networks, which promote their development and cell-specific functions. Using RT-qPCR, we further confirmed a robust, inverse relationship between decreased IR levels and spliced transcript expression in a select group of genes known to be important in macrophage differentiation (*ID2* and IRF7) and function (*TYMP*, *LAT* and *ENG*) (46–52). Collectively, these results show that transcripts important for macrophage development and function exhibit enhanced levels of IR in monocytes. This may allow monocytes to post-transcriptionally repress the inappropriate expression of these genes and proteins, while remaining poised for differentiation into macrophages.

Although a minority of transcripts increased in IR levels during monocyte-to-macrophage differentiation *in vitro*, we identified groups of genes strongly implicated in RNA processing and splicing. These IR-affected genes showed an inverse relationship between IR and gene/protein expression. Using RT-qPCR and mass spectrometry, we confirmed this observation in important RNA processing factors (*SNRPA1*, *HNRNPH1* and *THOC6*). Increased IR or the 'unproductive splicing' of RNA-binding and -splicing factors has been previously shown to decrease their expression, typically via NMD (6,55,67,68). This conserved mechanism allows cells to fine-tune homeostatic levels of splicing factors or to dramatically alter their expression during vital processes such as differentiation or activation. Our results show that a distinct cluster of RNA processing genes are subject to increased IR and decreased splice transcript expression during monocyte-to-macrophage differentiation. These intron-retaining transcripts are likely controlled independently of the major gene cluster exhibiting decreased IR, and may allow differentiating monocytes to post-transcriptionally repress RNA processing factors. Understanding how cells regulate separate pools of intron-retaining transcripts is an area which requires further study.

The mechanisms regulating the fate (i.e. retention vs degradation) of IR transcripts are poorly understood and are cell-type dependent. In contrast to previous reports (11,13,14), inhibition of cytoplasmic NMD via UPF1 knockdown did not result in the accumulation of intron-retaining transcripts in THP-1-derived Mϕ-like macrophages, indicating that they were not subject to NMD (Figure 2C and D). We further established that these transcripts were detained within the nucleus, explaining their protection from NMD, which occurs primarily during the pioneer round of translation in the cytoplasm (69). Similarly, in THP-1 monocytes, we observed significant nuclear detention of functionally important, intron-retaining transcripts *ID2*, *ENG* and *LAT*. This strongly suggests that IR coupled with nuclear detention and protection from decay is a mechanism employed by monocytes to facilitate timely expression of key regulators of macrophage development and function during differentiation. Such a finding differs substantially to what we previously established in granulocytes, in which IR was strongly linked to NMD (11). Although granulocytes and monocytes are derived from the same progenitor cell (GMP), they evidently show striking phenotypic differences in IR regulation during terminal differentiation. Granulocytes display an increase in IR coupled with cytoplasmic decay whilst macrophages display a general decrease in IR coupled with nuclear detention, which makes them similar to neurons, T cells and gametes (7–9,12).

It has been speculated that nuclear-detained, intron-retaining transcripts with downregulated spliced transcript expression are targets of the RNA exosome (9,10), as previously shown for a single example of genes that retained introns in neurons (12). However, after effectively knocking down both the level and activity of catalytic components of the nuclear RNA exosome (12,18,19) in macrophages, we observed little or no increase in IR globally and in our transcripts of interest. This indicates that nuclear detention of intron-retaining or unproductively spliced transcripts does not necessarily make them targets of the nuclear RNA exosome. Such transcripts may be differentially localised, have protective secondary structures, or are bound by proteins in the nucleus making them resistant to degradation through this pathway (19). Thus, our results suggest that macrophages process intron-retaining transcripts by a yet unknown nuclear RNA surveillance machinery. Approximately two-fifths of intron-retaining transcripts in monocytes and macrophages contributed to a total increase in transcript expression indicating that they may be protected from degradation and poised to trigger downstream biological functions (Figure 1H and I).

Our findings that *CXCL2* and *NFKBIZ* are regulated by IR during macrophage activation indicates that IR has an important role in the innate immune response. *CXCL2* and *NFKBIZ* transcripts undergo dramatic reductions in IR, which coincides with a robust upregulation of their spliced transcript expression. The rapid accumulation of intron-retaining *CXCL2* transcripts early during exposure to a proinflammatory stimulus is intriguing (Figure 6G). This observation agrees with the concept of RNA velocity, whereby cells start to increase transcription leading to an accumulation of unspliced transcripts. This prepares cells for a subsequent developmental/functional stage where the expression of fully-spliced transcripts is essential (70). In the case of an inflammatory response, stockpiling of intron-retaining *CXCL2* may be pivotal to ensure a 'volley' of chemokine release to effectively facilitate recruitment of granulocytes to the site of infection. Indeed, 1–3 hours after the accumulation of intron-retaining *CXCL2* transcripts, we observed substantial secretion of CXCL2 proteins concomitant with decreased IR over time (Figure 6G), further substantiating the role of IR in regulating the inflammatory response. Moreover, we established that a pool of mature, intron-retaining *CXCL2* and *NFKBIZ* is maintained in the nuclei of resting macrophages. Previous studies in mice have demonstrated that, following macrophage activation, there is a significant, but transient, increase in unspliced mRNA in the nucleus (71,72). A similar phenomenon may also occur in humans, whereupon transcriptional upregulation of proinflammatory genes is accompanied by increased IR and storage of nuclear transcripts. This may render macrophages poised for a rapid and potent response to microbial infection following *en masse* splicing and production of proinflammatory proteins. Using *CXCL2* as an example, this proposed model is summarised in Figure 7. Our results are consistent with the recently published role of nuclear detained intron-retaining transcripts as 'sentinel RNAs' that facilitate rapid protein synthesis, faster than *de novo* transcription and translation, when appropriate stimuli are present (7,8,17).

Overall, our comprehensive study provides novel insights into the role of IR during both monocyte-to-macrophage differentiation and macrophage activation. Monocytes and macrophages employ coordinated IR coupled with nuclear detention, to regulate the expression of important genes. Further investigation into the mechanisms that underpin this phenomenon will enable a better understanding of diseases characterised by aberrant macrophage function. For example, altered CXCL2 expression and signalling has been strongly implicated in a range of inflammatory pathologies, including those of the vasculature, lung, adipose tissue

and kidney (63,73–76). Thus, it may be possible to target CXCL2 and other proinflammatory proteins through modulation of the spliceosome, which is relevant for numerous immunological disorders (77).

DATA AVAILABILITY

mRNA sequencing and WGBS data that support the findings of this study have been deposited in Gene Expression Omnibus under the accession number GSE130011. RAW MS data have been deposited to the ProteomeXchange Consortium (http://proteomecentral.proteomexchange.org) via the PRIDE partner repository with the dataset identifier PXD017391.

SUPPLEMENTARY DATA

Supplementary Data are available at NAR Online.

ACKNOWLEDGEMENTS

We thank Rajini Nagarajah for technical assistance and Tara Roberts for reagents.
Author contributions: I.D.G. performed most of the experiments with critical contributions from N.P. Q.L., C.-T.K., A.C.H.W. and J.M.H. provided substantial assistance in the acquisition of cells and validation of results. R.S. and U.S. performed bioinformatics analyses. R.H performed Nanopore sequencing. M.L performed mass spectrometry and related data analyses. S.S.N. and S.J.C contributed to the whole genome bisulphite sequencing. B.R. provided critical input for the purification of monocyte and macrophage cells including the design of related experiments. I.D.G., J.E.J.R. and J.J.-L.W. designed the majority of experiments. J.J.-L.W. conceived the overall project and supervised its execution. I.D.G., N.P., B.R., J.E.J.R. and J.J.-LW wrote the manuscript with critical contributions from all co-authors. I.D.G. and N.P. contributed equally to the paper. We thank SydneyMS for providing the instrumentation used in this study.

FUNDING

National Health and Medical Research Council [1128175, 1129901 to J.E.J.R. and J.J.-L.W., 1126306 to J.J.-L.W., 1063559 to S.J.C.]; the Cancer Council of NSW [20-12 to U.S.]; NSW Genomics Collaborative Grant (to J.E.J.R. and J.J.-L.W.); Cure the Future (to J.E.J.R.); and an anonymous foundation (to J.E.J.R.); M.L., B.R., U.S. and J.J.-L.W. hold fellowships from the Cancer Institute of New South Wales; I.D.G. and A.C.H.W. are recipients of the Australian Government Research Training Program PhD Scholarships; N.P. is a recipient of the Sydney Catalyst Postgraduate Scholarship, NHMRC Postgraduate Scholarship and the Arrow Bone Marrow Transplant Foundation Supplementary PhD Scholarship. Funding for open access charge: National Health and Medical Research Council.
Conflict of interest statement. None declared.

REFERENCES

1. Licatalosi,D.D. and Darnell,R.B. (2010) RNA processing and its regulation: global insights into biological networks. *Nat . Rev. Genet.*, **11**, 75–87.
2. Nilsen,T. and Graveley,B.R. (2010) Expansion of the eukaryotic proteome by alternative splicing. *Nature*, **463**, 457–463.
3. Braunschweig,U., Barbosa-Morais,N.L., Pan,Q., Nachman,E.N., Alipanahi,B., Gonatopoulos-Pournatzis,T., Grey,B., Irimia,M. and Blencowe,B.J. (2014) Widespread intron retention in mammals functionally tunes transcriptomes. *Genome Res.*, **24**, 1774–1786.
4. Schmitz,U., Pinello,N., Jia,F., Alasmari,S., Ritchie,W., Keightley,M.-C., Shini,S., Lieschke,G.J., Wong,J.J.-L. and Rasko,J.E.J. (2017) Intron retention enhances gene regulatory complexity in vertebrates. *Genome Biol.*, **18**, 216.
5. Edwards,C.R., Ritchie,W., Wong,J.J.-L., Schmitz,U., Middleton,R., An,X., Mohandas,N., Rasko,J.E.J. and Blobel,G.A. (2016) A dynamic retention program in the mammalian megakaryocyte and erythrocyte lineages. *Blood*, **127**, e24–e34.
6. Llorian,M., Gooding,C., Bellora,N., Hallegger,M., Buckroyd,A., Wang,X., Rajgor,D., Kayikci,M., Feltham,J., Ule,J. *et al.* (2016) The alternative splicing program of differentiated smooth muscle cells involves concerted non-productive splicing of post-transcriptional regulators. *Nucleic Acids Res.*, **14**, 8933–8950.
7. Mauger,O., Lemoine,F. and Scheiffele,P. (2016) Targeted intron retention and excision for rapid gene regulation in response to neuronal activity. *Neuron*, **92**, 1266–1278.
8. Naro,C., Jolly,A., Di Persio,S., Bielli,P., Setterblad,N., Alberdi,A.J., Vicini,E., Geremia,R., De la Grange,P. and Sette,C. (2017) An orchestrated intron retention program in meiosis controls timely usage of transcripts during germ cell differentiation. *Dev. Cell*, **41**, 82–93.
9. Ni,T., Yang,W., Han,M., Zhang,Y., Shen,T., Nie,H., Zhou,Z., Dai,Y., Yang,Y., Liu,P. *et al.* (2016) Global intron retention mediated gene regulation during CD4+ T cell activation. *Nucleic Acids Res.*, **44**, 6817–6829.
10. Pimentel,H., Parra,M., Gee,S.L., Mohandas,N., Pachter,L. and Conboy,J.G. (2016) A dynamic intron retention program enriched in RNA processing genes regulates gene expression during terminal erythropoiesis. *Nucleic Acids Res.*, **44**, 838–851.
11. Wong,J.J.-L., Ritchie,W., Ebner,O.A., Selbach,M., Wong,J.W.H., Huang,Y., Gao,D., Pinello,N., Gonzalez,M., Baidya,K. *et al.* (2013) Orchestrated intron retention regulates normal granulocyte differentiation. *Cell*, **154**, 583–595.
12. Yap,K., Lim,Z.Q., Khandelia,P., Friedman,B. and Makeyev,E.V. (2012) Coordinated regulation of neuronal mRNA steady-state levels through developmentally controlled intron retention. *Genes Dev.*, **26**, 1209–1223.
13. Jaillon,O., Bouhouche,K., Gout,J.F., Aury,J.M., Noel,B., Saudemont,B., Nowacki,M., Serrano,V., Porcel,B.M., Ségurens,B. *et al.* (2008) Translational control of intron splicing in eukaryotes. *Nature*, **451**, 359–362.
14. Lykke-Andersen,S. and Jensen,T.H. (2015) Nonsense-mediated mRNA decay: an intricate machinery that shapes transcriptomes. *Nat. Rev. Mol. Cell Biol.*, **16**, 665–677.
15. Boutz,P.L., Bhutkar,A. and Sharp,P.A. (2015) Detained introns are a novel, widespread class of post-transcriptionally spliced introns. *Genes Dev.*, **29**, 63–80.
16. Boothby,T.C., Zipper,R.S., van der Weele,C.M. and Wolniak,S.M. (2013) Removal of retained introns regulates transition in the rapidly developing gametophyte of Marsilea vestita. *Dev. Cell*, **24**, 517–529.
17. Gill,J., Park,Y., McGinnis,J.P., Perez-Sanchez,C., Blanchette,M. and Si,K. (2017) Regulated intron removal integrates motivational state and experience. *Cell*, **169**, 836–848.
18. Lemieux,C., Marguerat,S., Lafontaine,J., Barbezier,N., Bähler,J. and Bachand,F. (2011) A pre-mRNA degradation pathway that selectively targets intron-containing genes requires the nuclear poly(A)-binding protein. *Mol. Cell*, **44**, 108–119.
19. Kilchert,C., Wittmann,S. and Vasiljeva,L. (2016) The regulation and functions of the nuclear RNA exosome complex. *Nat. Rev. Mol. Cell Biol.*, **17**, 227–239.
20. Ginhoux,F. and Jung,S. (2014) Monocytes and macrophages: Developmental pathways and tissue homeostasis. *Nat. Rev. Immunol.*, **14**, 392–404.

21. Pollard,J.W. (2009) Trophic macrophages in development and disease. *Nat. Rev. Immunol.*, **9**, 259–270.
22. Davies,L.C., Jenkins,S.J., Allen,J.E. and Taylor,P.R. (2013) Tissue-resident macrophages. *Nat. Immunol.*, **14**, 986–995.
23. Martinez,F.O., Gordon,S., Locati,M. and Mantovani,A. (2006) Transcriptional profiling of the human monocyte-to-macrophage differentiation and polarisation: New molecules and pattterns of gene expression. *J. Immunol.*, **177**, 7303–7311.
24. Schnoor,M., Buers,I., Sietmann,A., Brodde,M.F., Hofnagel,O., Robenek,H. and Lorkowski,S. (2009) Efficient non-viral transfection of THP-1 cells. *J. Immunol. Methods*, **344**, 109–115.
25. Chanput,W., Mes,J.J. and Wichers,H.J. (2014) THP-1 cell line: An in vitro cell model of immune modulation approach. *Int. Immunopharmacol.*, **23**, 37–45.
26. Dobin,A., Davis,C.A., Schlesinger,F., Drenkow,J., Zaleski,C., Jha,S., Batut,P., Chaisson,M. and Gingeras,T.R. (2013) STAR: ultrafast universal RNA-seq aligner. *Bioinformatics*, **29**, 15–21.
27. Middleton,R., Gao,D., Thomas,A., Singh,B., Au,A., Wong,J.J.-L., Bomane,A., Cosson,B., Eyras,E., Rasko,J.E.J. *et al.* (2017) IRFinder: assessing the impact of intron retention on mammalian gene expression. *Genome Biol.*, **18**, 51.
28. Love,M.I., Huber,W. and Anders,S. (2014) Moderated estimation of fold change and dispersion for RNA-seq data with DESeq2. *Genome Biol.*, **15**, 550.
29. Liu,H., Lorenzini,P.A., Zhang,F., Xu,S., Wong,M.S.M., Zheng,J. and Roca,X. (2018) Alternative splicing analysis in human monocytes and macrophages reveals MBNL1 as major regulator. *Nucleic Acids Res.*, **46**, 6069–6086.
30. Nair,S.S., Luu,P.-L., Maddugoda,M., Huschtscha,L., Reddel,R., Chenevix-Trench,G., Toso,M., Kench,J.G., Horvath,L.G., Hayes,V.M. *et al.* (2018) Guidelines for whole genome bisulphite sequencing of intact and FFPET DNA on the Illumina HiSeq X Ten. *Epigenet. Chromatin*, **11**, 24.
31. Wong,J.J.-L., Gao,D., Nguyen,T.B., Kwok,C.-T., van Geldermalsen,M., Middleton,R., Pinello,N., Thoeng,A., Nagarajah,R., Holst,J. *et al.* (2017) Intron retention is regulated by altered MeCP2-mediated splicing factor recruitment. *Nat. Commun.*, **8**, 15134.
32. Robinson,J.T., Thorvaldóttir,H., Winckler,W., Guttman,M., Lander,E.S., Getz,G. and Mesirov,J.P. (2011) Integrative Genomics Viewer. *Nat. Biotechnol.*, **29**, 24–26.
33. Tyner,C., Barber,G.P., Casper,J., Clawson,H., Diekhans,M., Eisenhart,C., Fischer,C.M., Gibson,D., Gonzalez,J.N., Guruvadoo,L. *et al.* (2017) The UCSC genome browser database: 2017 update. *Nucleic Acids Res.*, **45**, D626–D634.
34. O'Leary,A.A., Wright,M.W., Brister,J.R., Ciufo,S., Haddad,D., McVeigh,R., Rajput,B., Robbertse,B., Smith-White,B., Ako-Adjei,D. *et al.* (2015) Reference sequence (RefSeq) database at NCBI: current status, taxonomic expansion, and functional annotation. *Nucleic Acids Res.*, **44**, D733–D745.
35. Young,M.D., Wakefield,M.J., Smyth,G.K. and Oshlack,A. (2010) Gene ontology analysis for RNA-seq: accounting for selection bias. *Genome Biol.*, **11**, R14.
36. Li,H. (2018) Minimap2: pairwise alignment for nucleotide sequences. *Bioinformatics*, **34**, 3094–3100.
37. Harney,D.J., Hutchison,A.T., Hatchwell,L., Humphrey,S.J., James,D.E., Hocking,S., Heilbronn,L.K. and Larance,M. (2019) Proteomic analysis of human plasma during intermittent fasting. *J. Proteome Res.*, **18**, 2228–2240.
38. Cox,J. and Mann,M. (2008) MaxQuant enables high peptide identification rates, individualized p.p.b.-range mass accuracies and proteome-wide protein quantification. *Nat. Biotechnol.*, **26**, 1367–1372.
39. Cox,J., Neuhauser,N., Michalski,A., Scheltema,R.A., Olsen,J.V. and Mann,M. (2011) Andromeda: a peptide search engine integrated into the MaxQuant environment. *J. Proteome Res.*, **10**, 1794–1805.
40. Cox,J., Hein,M.Y., Luber,C.A., Paron,I., Nagaraj,N. and Mann,M. (2014) Accurate proteome-wide label-free quantification by delayed normalisation and maximal peptide ratio excretion, termed MaxLFQ. *Mol. Cell Proteomics*, **13**, 2513–2526.
41. Audic,S. and Claverie,J.M. (1997) The significance of digital gene expression profiles. *Genome Res.*, **7**, 986–995.
42. Rambaldi,A., Young,D.C. and Griffin,J.D. (1987) Expression of the M-CSF (CSF-1) gene by human monocytes. *Blood*, **69**, 1409–1413.
43. Auwerx,J. (1991) The human leukaemia cell line, THP-1: A multifaceted model for the study of monocyte-macrophage differentiation. *Experientia*, **47**, 22–31.
44. Wong,J.J.-L., Au,A.Y.M., Dadi,G., Pinello,N., Kwok,C.-T., Thoeng,A., Lau,K.A., Gordon,J.E.A., Schmitz,U., Feng,Y. *et al.* (2016) RBM3 regulates temperatures sensitive miR-142-5p and miR-143 (thermomiRs), which target immune genes and control fever. *Nucleic Acids Res.*, **44**, 2888–2897.
45. de Bruin,R.G., Shiue,L., Prins,J., de Boer,H.C., Singh,A., Fagg,W.S., van Gils,J.M., Duijs,J.M.G.J., Katzman,S., Kraaijeveld,A.O. *et al.* (2016) Quaking promotes monocyte differentiation into pro-atherogenic macrophages by controlling pre-mRNA splicing and gene expression. *Nat. Commun.*, **7**, 10846.
46. Ishiguro,A., Spirin,K.S., Shiohara,M., Tobler,A., Gombart,A.F., Israel,M.A., Norton,J.D. and Koeffler,H.P. (1996) Id2 expression increases with differentiation of human myeloid cells. *Blood*, **87**, 5225–5231.
47. Kawahara,A., Hattori,S., Akiba,J., Nakashima,K., Taira,T., Watari,K., Hosoi,F., Uba,M., Basaki,Y., Koufuji,K. *et al.* (2010) Infiltration of thymidine phosphorylase-positive macrophages is closely associated with tumor angiogenesis and survival in intestinal type gastric cancer. *Oncol. Rep.*, **24**, 405–415.
48. Tridandapani,S., Lyden,T.W., Smith,J.L., Carter,J.E., Coggeshall,K.M. and Anderson,C.L. (2000) The adapter protein LAT enhcances Fcγ receptor-mediated signal transduction in myeloid cells*. *J. Biol. Chem.*, **275**, 20480–20487.
49. Ojeda-Fernández,L., Recio-Poveda,L., Aristorena,M., Lastres,P., Blanco,F.J., Sanz-Rodriguez,F., Gallardo-Vara,E., de las Casas-Engel,M., Corbí,Á., Arthur,H.M. *et al.* (2016) Mice lacking endoglin in macrophages show an impaired immune response. *PloS Genet.*, **12**, e1005935.
50. Scharpfenecker,M., Floot,B., Russell,N.S. and Stewart,F.A. (2012) The TGF-β co-receptor endoglin regulates macrophage infiltration and cytokine production in the irradiated mouse kidney. *Radiother. Oncol.*, **105**, 313–320.
51. Lu,R. and Pitha,P.M. (2001) Monocyte differentiation to macrophage requires interferon regulatory factor 7. *J. Biol. Chem.*, **276**, 45491–45496.
52. Ning,S., Pagano,J.S. and Barber,G.N. (2011) IRF7: activation, regulation, modification and function. *Genes Immun.*, **12**, 399–414.
53. Grammatikakis,I., Zhang,P., Panda,A.C., Kim,J., Maudsley,S., Abdelmohsen,K., Yang,X., Martindale,J.L., Motiño,O., Hutchison,E.R. *et al.* (2016) Alternative splicing of neuronal differentiation factor TRF2 regulated HNRNPH1/H2. *Cell Rep.*, **15**, 926–934.
54. Masuda,S., Das,R., Cheng,H., Hurt,E., Dorman,N. and Reed,R. (2005) Recruitment of the human TREX complex to mRNA during splicing. *Genes Dev.*, **19**, 1512–1517.
55. Lareau,L.F., Inada,M., Green,R.E., Wengrod,J.C. and Brenner,S.E. (2007) Unproductive splicing of SR genes associated with highly conserved and ultraconserved DNA elements. *Nature*, **446**, 926–929.
56. Tripathi,V., Ellis,J.D., Shen,Z., Song,D.Y., Pan,Q., Walt,A.T., Freier,S.M., Bennet,C.F., Sharma,A., Bubulya,P.A. *et al.* (2010) The nuclear-retained noncoding RNA MALAT1 regulates alternative splicing by modulating SR splicing factor phosphorylation. *Mol. Cell*, **39**, 925–938.
57. Wasmuth,E.V., Januszyk,K. and Lima,C.D. (2014) Structure of an Rrp6-RNA exosome complex bound to poly(A) RNA. *Nature*, **511**, 435–439.
58. Preker,P., Nielsen,J., Kammler,S., Lykke-Andersen,S., Christensen,M.S., Mapendano,C.K., Schierup,M.H. and Jensen,T.H. (2008) RNA exosome depletion reveals transcription upstream of active human promoters. *Science*, **322**, 1851–1854.
59. Szczepińska,T., Kalisiak,K., Tomecki,R., Labno,A., Borowski,L.S., Kulinski,T.M., Adamska,D., Kosinska,J. and Dziembowski,A. (2015) DIS3 shapes the RNA polymerase II transcriptome in humans by degrading a variety of unwanted transcripts. *Genome Res.*, **25**, 1622–1633.
60. Genin,M., Clement,F., Fattaccioli,A., Raes,M. and Michiels,C. (2015) M1 and M2 macrophages derived from THP-1 cells differentially modulate the response of cancer cells to etoposide. *BMC Cancer*, **15**, 577.
61. Jablonski,K.A., Amici,S.A., Webb,L.M., de Dios Ruiz-Rosado,J., Popovich,P.G., Partida-Sanchez,S. and Gureau-de-Arellano,M.

(2015) Novel markers to delineate murine M1 and M2 macrophages. *PloS One*, **10**, e0145342.
62. Zhou,D., Chen,L., Yang,K., Jiang,H., Xu,W. and Luan,J. (2017) SOCS molecules: the growing players in macrophage polarisation and function. *Oncotarget*, **8**, 60710–60722.
63. De Filippo,K., Dudeck,A., Hasenberg,M., Nye,E., van Rooijen,N., Hartmann,K., Gunzer,M., Roers,A. and Hogg,N. (2013) Mast cell and macrophage chemokines CXCL1/CXCL2 control the early stage of neutrophil recruitment during tissue inflammation. *Blood*, **121**, 4930–4937.
64. Hörber,S., Hildebrand,D.G., Lieb,W.S., Lorscheid,S., Hailfinger,S., Schulze-Osthoff,K. and Essman,F. (2016) The atypical inhibitor of NF-κB, IκBζ, controls macrophage interleukin-10 expression*. *J. Biol. Chem.*, **291**, 12851–12861.
65. Herzel,L., Starube,K. and Neugebauer,K.M. (2018) Long-read sequencing of nascent RNA reveals coupling among RNA processing events. *Genome Res.*, **28**, 1008–1019.
66. Oesterreich,F.C., Herzel,L., Straube,K., Hujer,K., Howard,J. and Neugebauer,K.M. (2016) Splicing of nascent RNA coincides with intron exit from RNA polymerase II. *Cell*, **165**, 372–381.
67. Lareau,L.F. and Brenner,S.E. (2015) Regulation of splicing factors by alternative splicing and NMD is conserved between kingdoms yet evolutionarily flexible. *Mol. Biol. Evol.*, **32**, 1072–1079.
68. Ni,J.Z., G.,L., Donohoe,J.P., Preston,C., Nobida,N., O'Brien,G., Shiue,L., Clark,T.A., Blume,J.E. and Ares,M. Jr (2007) Ultraconserved elements are associated with homeostatic control of splicing regulators by alternative splicing and nonsense-mediated decay. *Genes Dev.*, **21**, 708–718.
69. Trcek,T., Sato,H., Singer,R.H. and Maquat,L.E. (2013) Temporal and spatial characterization of nonsense-mediated mRNA decay. *Genes Dev.*, **27**, 541–551.
70. La Manno,G., Soldatov,R., Zeisel,A., Braun,E., Hochgerner,H., Petukhov,V., Lidschreiber,K., Kastriti,M.E., Lönnerberg,P., Furlan,A. *et al.* (2018) RNA velocity of single cells. *Nature*, **560**, 494–498.
71. Bhatt,D.M., Pandya-Jones,A., Tong,A.J., Barozzi,I., Lissner,M.M., Natoli,G., Black,D.L. and Smale,S.T. (2012) Transcript dynamics of proinflammatory genes revealed by sequence analysis of subcellular RNA fractions. *Cell*, **150**, 279–290.
72. Pandya-Jones,A., Bhatt,D.M., Lin,C.-H., Tong,A.-J., Smale,S.T. and Black,D.L. (2013) Splicing kinetics and transcript release from the chromatin compartment limit the rate of lipid A-induced gene expression. *RNA*, **19**, 811–827.
73. Girbl,T., Lenn,T., Perez,L., Rolas,L., Barkaway,A., Thiriot,A., Del Fresno,C., Lynam,E., Hub,E., Thelen,M. *et al.* (2018) Distinct compartmentalisation of the chemokines CXCL1 and CXCL2 and the atypical receptor ACKR1 determine discrete stages of neutrophil diapedesis. *Immunity*, **49**, 1062–1076.
74. Al-Alwan,L.A., Chang,Y., Mogas,A., Halayko,A.J., Baglole,C.J., Martin,J.G., Rousseau,S., Eidelman,D.H. and Hamid,Q. (2013) Differential roles of CXCL2 and CXCL3 and their receptors in regulating normal and asthmatic airway smooth muscle cell migration. *J. Immunol.*, **195**, 2731–2741.
75. Rouault,C., Pellegrinelli,V., Schlich,R., Cotillard,A., Poitou,C., Tordjman,J., Sell,H., Clément,K. and Lacasa,D. (2013) Roles of chemokine ligand-2 (CXCL2) and neutrophils in influencing endothelial cell function and inflammation of human adipose tissue. *Endocrinology*, **154**, 1069–1079.
76. Roche,J.K., Keepers,T.R., Gross,L.K., Seaner,R.M. and Obrig,T.G. (2007) CXCL1/KC and CXCL2/MIP-2 are critical effectors and potential targets for therapy of Escherichia coli O157:H7-associated renal inflammation. *Am. J. Pathol.*, **170**, 526–537.
77. Arechavala-Gomeza,V., Khoo,B. and Aartsma-Rus,A. (2014) Splicing modulation therapy in the treatment of genetic diseases. *Appl. Clin. Genet.*, **7**, 245–452.